SAND2020-3761J

Corrosion and Mechanical Performance of Grade 92 Ferritic-Martensitic Steel After Exposure to Supercritical Carbon Dioxide

ANDREW BRITTAN, JACOB MAHAFFEY, and MARK ANDERSON

Grade 92 ferritic-martensitic steel is a candidate alloy for medium temperature (< 550 °C) components for the supercritical carbon dioxide (s-CO_2) Brayton cycle. 1000 hours exposures were performed on base and welded material in s-CO_2 at temperatures of 450 °C or 550 °C and compared to samples aged in Ar at 550 °C. Both s-CO_2 exposures resulted in a duplex oxide growth and carburization, with 450 °C exhibiting carburization in a power law diffusion profile up to a depth of 200-250 μm, while 550 °C showed a linear profile up to a depth of 100 μm. The different profiles indicate much slower precipitation and coarsening of carbides at the lower temperature, allowing carbon to diffuse deeper into the material. However, 450 °C produced improved mechanical properties while 550 °C produced deteriorated properties. This was due to the higher density of carbon near the metal–oxide interface which leads to significant carbide coarsening and, subsequently, crack initiation and early failure. Additional exposure at 450 °C is predicted to increase deposited carbon, but further study would be needed to understand if and when carburization will produce a negative mechanical effect.

https://doi.org/10.1007/s11661-020-05691-7

I. INTRODUCTION

THE supercritical carbon dioxide (s-CO_2) Brayton cycle is currently being considered for next-generation power systems for uses across nuclear, solar, and fossil power sources. Compared to the current industry standard, the Rankine cycle, the Brayton cycle has been found to produce higher efficiencies at comparable operating temperatures.[1,2] Implementing an s-CO_2 Brayton cycle, however, will not be possible without a thorough understanding of the effects of the environment on candidate materials.[3]

Grade 92 ferritic-martensitic steel (P92 or NF616)—along with other 9-12 pct Cr ferritic steels—is being considered for medium temperature applications due to its good strength and creep properties up to its highest suggested service temperature of 620 °C.[4–10] These high-temperature properties are a result of precipitation of $M_{23}C_6$ carbides and MX carbonitrides along grain boundaries. A homogeneous distribution of these precipitates nucleates and remains relatively small during initial heat treatment of P92, due to the stabilizing effect of W.[11,12] The stabilization of precipitates causes no detrimental coarsening after further aging at 600 °C. However, after 1000 hours of aging at 600 °C Laves-phase precipitates and coarsens to above 0.5 μm, resulting in embrittlement, though the effect of this on creep strength is not confirmed.[7,13]

The mechanical properties of 9-12 pct Cr ferritic steels are highly dependent on the size, density, distribution, and morphology of both strengthening precipitates.[5] The P92 microstructure consists of 30–50 μm prior-austenite grains which are transformed during the heat treatment process to a dual phase structure of ferrite and tempered martensite, resulting in a grain size of 1-10 μm.[14] This fine grain structure allows for high strength from the near-homogeneous precipitation of strengthening precipitates along grain boundaries. Carbonitrides are not expected to significantly coarsen with additional carbon deposition, as they are likely limited by the availability of their forming metals, trace alloying elements V and Nb. Conversely, the forming metals of $M_{23}C_6$ carbides are primary alloying constituents (Fe, Cr, W, and Mo). The abundance of these constituents leads to enhanced coarsening when carbon is added to the matrix, in this case by environmental exposure to CO_2.[15–18] Additionally, the refined microstructure of P92 creates a dense network of diffusion pathways for carbon, potentially enhancing the depth-dependent

ANDREW BRITTAN is with the University of Wisconsin-Madison, 1500 Engineering Drive, Madison, WI, 53706 and also with the Oregon State University, 1891 SW Campus Way, Corvallis, OR, 97331. Contact e-mail: brittana@oregonstate.edu JACOB MAHAFFEY is with the Sandia National Laboratory, Albuquerque, NM, 87123. MARK ANDERSON is with the University of Wisconsin-Madison.

Manuscript submitted October 10, 2019.

Published online: 25 February 2020

effects of carburization when exposed to the CO_2 environment.

Oxidation of P92 and similar 9-12 pct Cr steels in CO_2 has been shown to result in a duplex oxide, with an outer magnetite and inner Fe-Cr spinel (with an average stoichiometry of $Fe_{2.3}Cr_{0.7}O_4$).[19,20] Once this duplex structure has developed, the alloy exists in a pseudo-steady-state, and further oxidation can be understood through the available space model.[21] This model describes a process by which Fe ions diffuse to the surface to oxidize into magnetite (Fe_3O_4) and hematite (Fe_2O_3). The diffusion of Fe results in vacancies near the oxide–metal interface, which coalesce into voids. Further, the growth of the magnetite and hematite results in porosity through which gaseous CO_2 can flow to the oxide–metal interface [22] where these voids then allow "available space" for internal oxidation of Fe and Cr.

It is believed that the internal oxidation to create the inner Fe-Cr spinel locally lowers the pO_2 to the point that Cr oxidizes preferentially.[19,20] In P91, a very similar 9 pct Cr steel, small islands of Cr-oxide have been observed underneath the inner Fe-Cr spinel, forming the internal oxidation zone (IOZ).[9] After exposure at 600 °C for 20,000 hours, P91 exhibited an IOZ characterized by chromite ($FeCr_2O_4$) and $M_{23}C_6$ carbides which had left the nearby matrix nearly devoid of Cr. The oxides were preferentially situated nearer the oxide–metal interface than the carbides. The indication is that internal carbides were formed, removing Cr from the matrix and isolating it in islands which were then oxidized as the oxide grew inward, thanks to the higher thermodynamic stability of the oxide. The removal of Cr from the surrounding matrix would then lead to oxidation of Fe (once the local pO_2 increases sufficiently) around the chromite islands to form the full Fe-Cr spinel with the above-listed average stoichiometry. This process is also likely to occur at lower temperatures and be very similar in P92.

Several experimental studies have been performed which exposed P91 or P92 to high-temperature CO_2. Previous work at the University of Wisconsin-Madison showed that P92 exposed to CO_2 at 450 °C, 20 MPa for 1000 hours produced an oxide layer of roughly 8 μm thickness, and carburization to a depth of up to 200 μm from the surface.[15] Another study exposed P91 to CO_2 at 550 °C, 25 MPa for 310 hours and discovered carbon contents between 1.5 and 2.0 atomic percent extending from the inner Fe-Cr spinel out beyond 50 μm (maximum reported depth of measurement).[19] A study at the National Energy Technology Laboratory exposed P91 to several different environments at 550 °C, and found 1500 hours of s-CO_2 exposure resulted in a roughly 37-μm-thick duplex oxide.[23] An additional study exposed P92 to an Ar-CO_2 50/50 mixture at 550 °C for up to 150 hours and found a carburized region of roughly 100 μm.[18]

The carburization and oxidation processes that occur in alloys exposed to CO_2 have been linked.[17,18,24] This is believed to be the result of the Boudouard reaction, given in (1). The direct reduction of CO_2 produces CO, and the recombination of two CO molecules into CO_2 produces an excess carbon atom. Therefore, the more oxidation that occurs, the greater the effect of carburization on the material. In addition, as internal oxidation occurs, previously formed carbides will get oxidized (oxides are generally more thermodynamically stable in pure CO_2 environments[25]) and create additional free carbon. In this way, the carbon profile will get pushed inward, and build up in and near the internal Fe-Cr spinel. The IOZ, meanwhile, has been shown to be carbon-poor, with the assumption being that as carbides are oxidized, the carbon is freed up and diffuses inward to find additional Cr to form carbides.[9] As discussed above, the coarsening of carbides should have a measurable effect on mechanical properties.

$$CO_2 + C \leftrightarrow 2CO \quad [1]$$

II. EXPERIMENTAL PROCEDURE

P92 base material was acquired from Anderson Laboratories, and 9CRWV-TIG filler[26] was purchased from Euroweld Limited. Material compositions are given in Table I. Welding was performed on 3.18 mm plates with a preheat-interpass temperature above 200 °C to avoid hydrogen-assisted cold cracking.[26] The weldment was then given a post-weld heat treatment (PWHT) of 765 °C/2.5 h in accordance with the boiler and pressure vessel code case 2179-8.[27] The plate was milled to 1.6-mm thickness to remove surface effects, and samples were produced using electrical discharge machining.

Tensile samples, previously described,[28] were cut transverse to the weld, with ellipsoidal corrosion samples taken from the area between the gauges of neighboring tensile samples. Samples were polished to 800-grit using SiC polishing paper prior to either unexposed tensile testing or exposure. The exposure facility utilized in this experiment has previously been described.[24,29,30] Exposures were performed for 1000 h in either research grade CO_2 (99.999 pct pure) at 450 °C or 550 °C, 20 MPa, or were aged in ultra-high purity Ar (99.999 pct pure) at 550 °C, 0.02 MPa. For base material, three samples were tested in the as-received heat-treated condition, while three were tested in each of 550 °C-exposed conditions and two were tested after 450 °C CO_2 exposure. For welded samples, six samples were tested after PWHT, while three were tested in each of the CO_2-exposed conditions and one after aging in Ar.

Tensile testing was performed at room temperature, and stress data were acquired from a MTS Criterion 43 with a 5 kN load cell. Strain data were acquired from a custom video extensometer setup which was verified to an accuracy of 1.2 pct for the Young's Modulus and a median difference per tensile measurement of 3 pct relative to an off-the-shelf extensometer on larger samples. Mass measurements were made both before and after exposure using a high-precision Sartorius scale with an accuracy of ± 2 μg. Samples were analyzed using a field-emission scanning electron microscope (FE-SEM) combined with energy-dispersive

spectroscopy (EDS), which included measuring oxide thickness. Elemental depth profiles were acquired using a Horiba GD Profiler 2—a glow-dispersion optical emission spectrometer (GD-OES)—and the sputtering depth was calibrated using a Zygo NewView 6K profilometer.

III. RESULTS

A. *Mass Change and Oxide Analysis*

The change in mass demonstrated the increased corrosion expected from 550 °C CO_2 exposure relative to that of 450 °C. The mass gains for base material were 4.950 ± 0.007 mg/cm^2 for 550 °C exposure and 1.429 ± 0.031 mg/cm^2 for 450 °C. For welded samples, mass gains were 4.508 ± 0.675 mg/cm^2 for 550 °C exposure and 1.541 ± 0.042 mg/cm^2 for 450 °C. The mass gain from 550 °C exposure was consistent with previous work.[23,31] Oxide thicknesses were determined using SEM images of cross-sectioned samples, as observed in Figures 1(a) and (c). Samples exposed to CO_2 at 450 °C exhibited an average thickness of 11.7 ± 1.7 μm, while those exposed at 550 °C resulted in an average of 36.9 ± 2.8 μm. These results indicate two things: there was no statistical difference in corrosion between welded and base material, and roughly three times as much corrosion occurred in CO_2 at 550 °C than at 450 °C.

Additionally, both exposures produced a duplex oxide consisting of an outer Fe-oxide layer and an inner Fe-Cr spinel, see Figure 2. The outer magnetite appears to have grown outward from the surface with a measured porosity of roughly 4-10 pct (through image processing). The inner Fe-Cr spinel, meanwhile, appears to have grown inward and contained no large pores. The inward and outward growth of these oxides is evident from both the composition of the oxides (trace alloying elements evident within the inner oxide but not the outer oxide) and the flat line separating the oxides (representing the original alloy surface). This confirms the characterization of the duplex oxide from the previous works mentioned above.[9,20,23]

As the Fe-Cr spinel is theorized to have grown inward, its thickness was measured to account for total material loss by the gauge cross-section of the tensile samples. The Fe-Cr spinel was found to average 4.2 ± 0.5-μm-thick after 450 °C exposure, and 12.2 ± 0.7 μm

Table I. Composition of Base and Filler Material Used in this Work

	Cr	W	Mo	Mn	Ni	V	C	Si	Nb	N	Al	P	S	B	Fe
Base Material	8.94	1.91	0.50	0.45	0.21	0.20	0.11	0.10	0.08	0.047	0.016	0.016	0.003	0.001	bal.
Filler Metal (9CrWV-TIG)	9.04	1.65	0.41	0.68	0.49	0.17	0.092	0.22	0.062	0.058	0.007	0.009	0.010	0.003	bal.

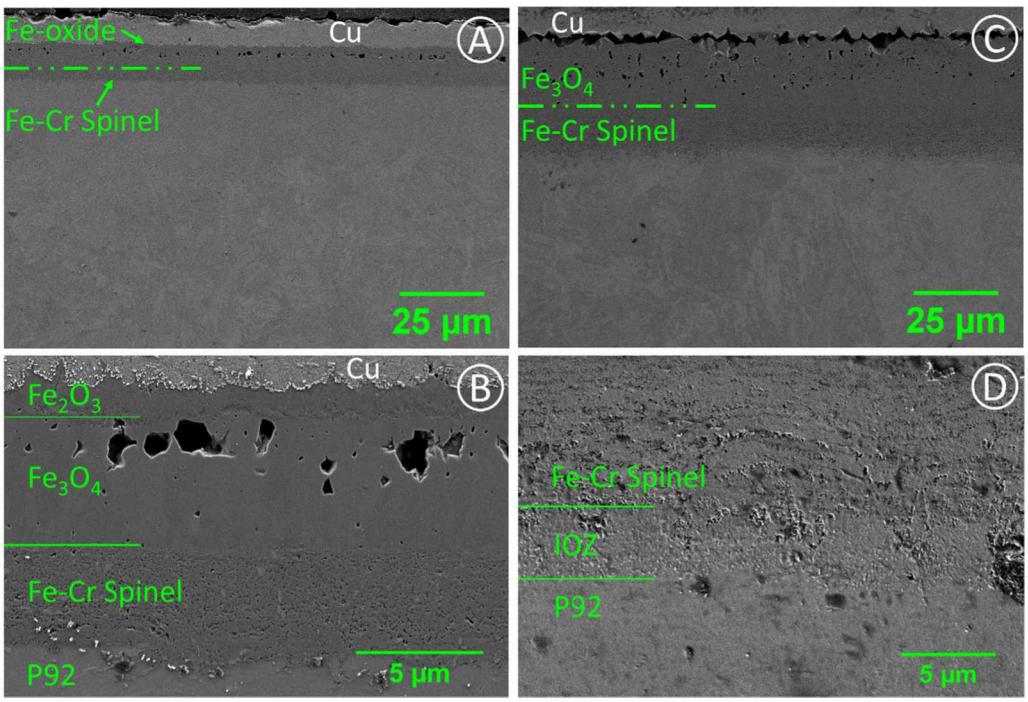

Fig. 1—Oxide of P92 exposed for 1000 h to CO_2 at 450 °C (*a*, *b*) and 550 °C (*c*, *d*) showing a duplex oxide formation of an outer Fe-oxide and an inner Cr-rich spinel. High-magnitude images (*b*, *d*) show that 450 °C exposure allows for a ~ 1-μm-thick layer of hematite above the magnetite (not observed at 550 °C), while the IOZ after 1000-h exposure at 550 °C is large enough to be observed (~ 3 μm thick).

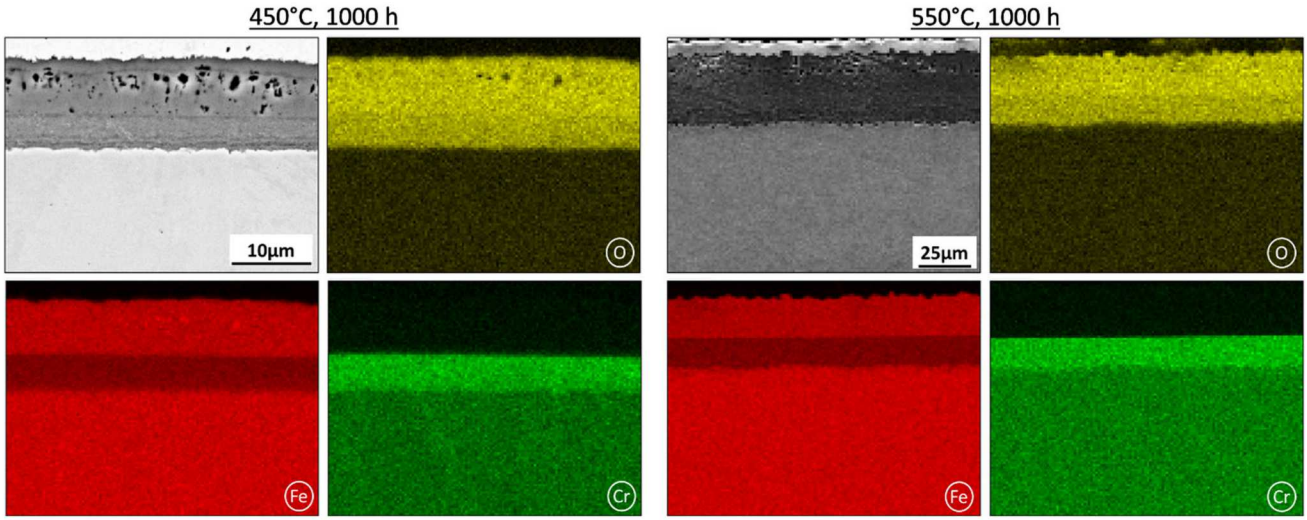

Fig. 2—EDS maps for the oxide from 450 °C and 550 °C, 1000 h exposures. Shows duplex oxide growth for both exposures: external Fe-oxide and internal Fe-Cr spinel.

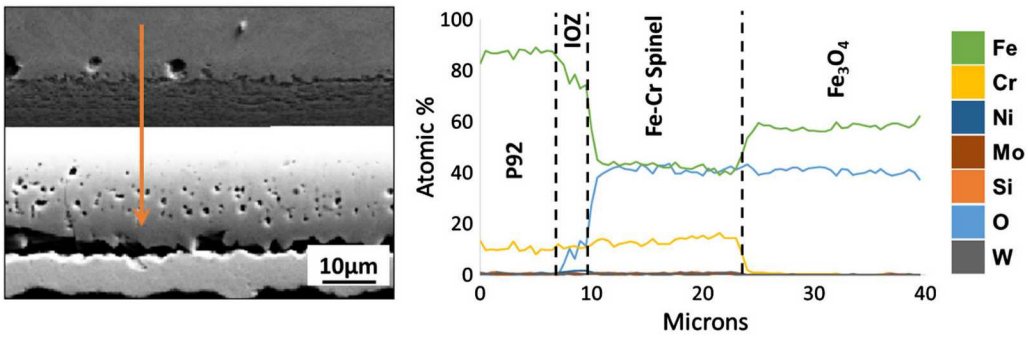

Fig. 3—EDS line scan over the oxide of a P92 sample exposed to CO_2 at 550 °C, 20 MPa for 1000 h. Shows the duplex oxide and the formation of a roughly 3-μm-thick IOZ.

after 550 °C exposure, corresponding to a 1 pct and 3 pct metal loss, respectively. This indicates that metal loss likely does not contribute to a significant loss in measured strength or ductility after exposure at either temperature.

The oxide morphology was different between the two 1000 hours CO_2 exposures. 450 °C exposure resulted in a 1-μm-thick layer of hematite above the magnetite, see Figure 1(b). Hematite was not observed after 550 °C exposure, likely due to rapid diffusion of Fe outward, removing the oxygen-rich phase quickly and keeping it too thin to observe with SEM. Further, Figures 1(d) and 3 show that 550 °C exposure allowed for the development of a ~ 3-μm-thick IOZ. This region was not large enough to be seen with SEM in the 450 °C-exposed samples, though it has been observed previously.[15]

B. *Tensile Results*

Tensile results, given in Table II, indicate strengthening occurred after both CO_2 exposures, for both welded and base material. For base material, 450 °C resulted in an 18 pct increase in yield strength (YS) and a 9 pct increase in ultimate tensile strength (UTS). The measured decrease in elongation is statistically insignificant due to the large variance in the measured quantities, indicating no significant drop in elongation. Meanwhile, the samples exposed to CO_2 at 550 °C experienced moderate increases in YS and UTS—3 pct and 6 pct, respectively—with a 35 pct loss in elongation relative to unexposed. In contrast to this, there was no observed mechanical effects of the inert environment thermal aging at 550 °C, an effect which has been seen before,[32] and indicates that laves-phase precipitates did not grow to a mechanically detrimental level.[7]

Welded samples exhibited similar results. 450 °C exposure in CO_2 resulted in a 17 pct increase in YS and a 6 pct increase in UTS, with only a 7 pct drop in elongation relative to unexposed. Exposure to CO_2 at 550 °C resulted in a negligible effect on YS and a 6 pct increase in UTS, with a drop in elongation of 29 pct. This is a very similar effect to that of base material: while 450 °C exposure increases strength with little or no cost in ductility, CO_2 exposure at 550 °C begins to have a negative effect on mechanical properties. In another similar result to that of base material, neutral aging at

Table II. Tensile Results for P92 Samples After the Given Exposure

	UTS (MPa)	0.2 pct YS (MPa)	Elongation (Pct)	Failure Location
Base: Unexposed	722 ± 4	562 ± 5	20.7 ± 0.5	N/A
Base: 450 °C CO_2	785 ± 5	664 ± 4	18.1 ± 4.3	N/A
Base: 550 °C CO_2	766 ± 2	577 ± 3	13.4 ± 0.6	N/A
Base: 550 °C Aging	735 ± 2	560 ± 1	19.9 ± 0.3	N/A
Welded: Unexposed	669 ± 1	509 ± 10	15.7 ± 0.2	FG-HAZ
Welded: 450 °C CO_2	709 ± 3	593 ± 10	14.6 ± 0.2	FG-HAZ
Welded: 550 °C CO_2	711 ± 3	518 ± 7	11.2 ± 0.6	FG-HAZ
Welded: 550 °C Aging	674	496	15.1	FG-HAZ

550 °C resulted in no meaningful change in tensile properties. All samples appeared to fail in the heat-affected zone (HAZ), likely in the fine-grained HAZ (FG-HAZ), which has previously been identified as a weak point in P92 welds,[33] and this was not altered by exposure.

The tensile results show that welded samples were consistently weaker and less ductile than base material. However, both welded and base samples exhibited the same response to exposure relative to the unexposed condition. This shows that the welding did not impact the mechanical response to either thermal aging or the s-CO_2 environment for P92. Welded samples also mirrored the results of mass change and oxide thickness compared to base material, so it can be determined that the effect of the s-CO_2 environment was the same. Therefore, the differences between base and welded samples will not be commented on in the following sections, as the analysis would be redundant.

C. *Fracture Surface Analysis*

Qualitative analysis was performed on pulled samples by examining the fracture surface after tensile testing of base material. As can be seen in Figure 4(a), unexposed P92 exhibited necking of the gauge, corresponding to the ductility observed after peak stress in the stress–strain curve. Figure 4(b) shows that the fracture surface was composed of a majority of micro-void coalescence (MVC), with micron-scale dimples, as well as some brittle cleavage, each corresponding to the microstructural phases, soft ferrite and hard martensite, respectively. Aging at 550 °C for 1000 hours did not change the fracture mode, as can be seen in Figures 4(a) and (d). The exposure of base material to CO_2 at 450 °C for 1000 hours resulted in a similar, though slightly different, fracture surface. Figures 4(e) and (f) show slightly less necking (image taken from the less ductile of the two samples), along with a similar mixture of micron-scale dimples and cleavage. The shared mode of fracture between unexposed, 550 °C aged, and 450 °C CO_2-exposed samples indicates that the ductility of the material did not change significantly from either exposure.

As seen in Figure 5, analysis of the samples exposed to CO_2 at 550 °C showed an altered fracture surface. Little-to-no localized necking was observed,

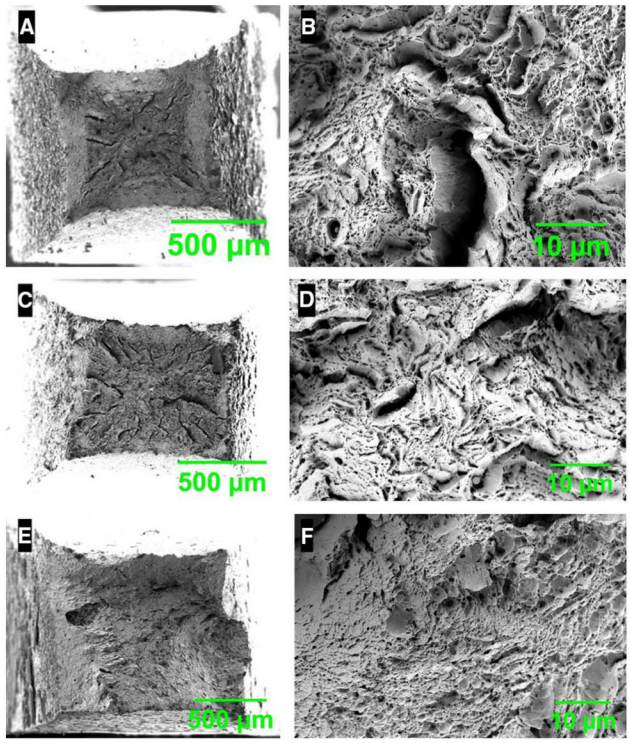

Fig. 4—Fracture surface images for P92 base material ruptured unexposed (*a*, *b*) and after neutral aging at 550 °C (*c*, *d*) show a mixture of micron-sized dimples (MVC) and cleavage, combined with overall sample necking. Fracture surface images for CO_2 exposed at 450 °C (*e*, *f*) show a similar mixture of MVC and cleavage, with decreased sample necking corresponding to lowered elongation observed in this sample.

corresponding to the lowered elongation in the tensile results. In addition, while there was still a mixture of MVC and cleavage, the sample cross-section was divided into roughly equal regions in which MVC dominated (Figure 5(b)) and cleavage dominated (Figure 5(c)). These regions were not depth-dependent, though the cleavage-dominated regions always had a connection to the edge of the sample. It is possible—even likely—that they were the result of near-surface crack initiation which then propagated along grain boundaries into the material until the true stress on the remaining area increased sufficiently to induce complete fracture.

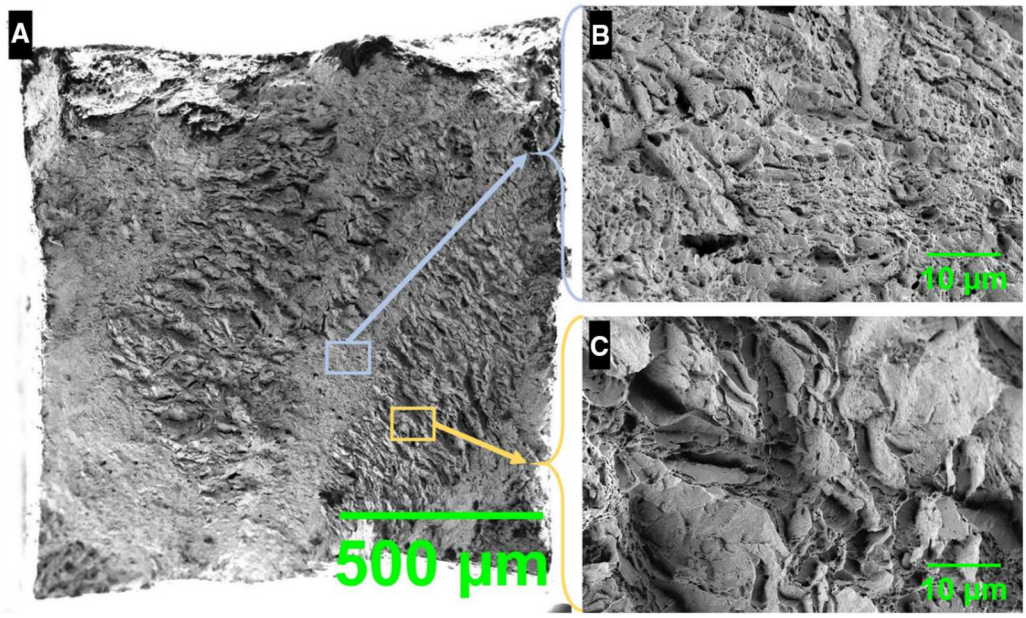

Fig. 5—Fracture surface images for CO_2-exposed base material at 550 °C. Characterized by very little necking (*a*), as well as regions dominated by a roughly even split of regions dominated by MVC (*b*) and cleavage (*c*).

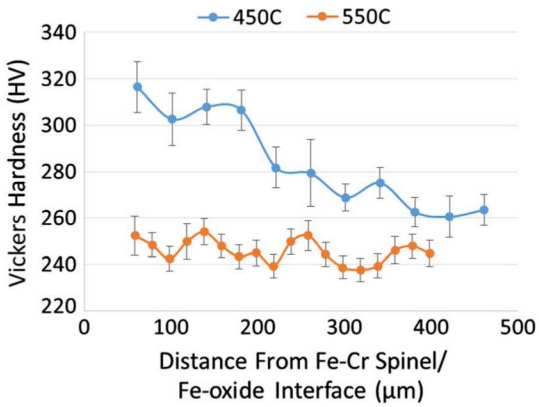

Fig. 6—Micro-hardness measurements near oxide after CO_2 exposure.

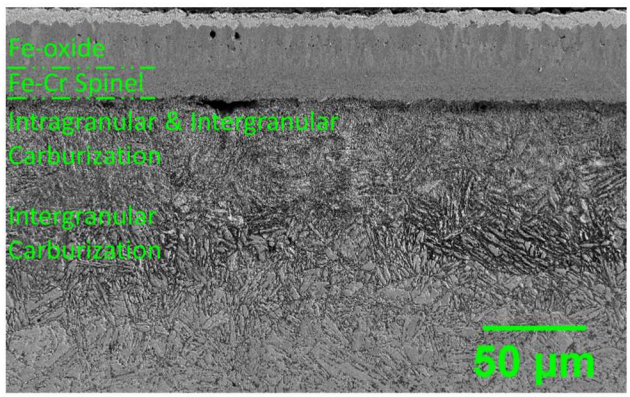

Fig. 7—Etched P92 base material after exposure to CO_2 at 550 °C, 20 MPa for 1000 h. Shows a carburization depth of 100-125 μm below a ~ 35 μm-thick-oxide.

D. *Carburization Analysis*

Micro-hardness measurements were obtained for both CO_2-exposure conditions and for unexposed samples, as it has been shown to be indicative of local carburization.[15] Bulk hardness measurements were made by averaging 25 measurements at the center of the sample (away from corrosion effects, as will be seen below), while depth measurements, given in Figure 6, were made by averaging 2-4 measurements equidistant from the interface between the inner and outer oxides. Bulk measurements found CO_2 exposure at 550 °C resulted in 241.2±5.1 HV, while 450 °C resulted in 252.8 ± 5.5 HV. In addition, the bulk of 550 °C aged P92 was found to have a hardness of 239.2 ± 5.2 HV. These match the hardness values reported in literature for heat-treated P92, which are in the range of 240-275 HV,[5,6] and indicate no effects of CO_2 in the bulk material. Depth measurements, however, shown in Figure 6, indicate that after exposure to 450 °C there is an increased hardness profile near the surface, which decays to the bulk values around 200–250 μm from the surface. A similar study has correlated this hardness profile to the magnitude and depth of carburization after exposure at 450 °C.[15] The 550 °C exposure, however, does not share this profile; the hardness of each point matched the bulk hardness. This indicates that either carbon did not penetrate to the minimum depth required for micro-hardness measurements, or the interaction of carbon was different during 550 °C exposure.

To investigate this disparity in hardness profiles, P92 was cross-sectioned and etched with 5 pct nitric acid in ethanol (5 pct Nital), shown Figure 7. Etching revealed a carburization depth below the oxide of 100-125 μm (135-160 μm below the surface) after exposure to CO_2 at 550 °C for 1000 hours. This depth is less than that seen here and reported previously for 450 °C exposure.[15]

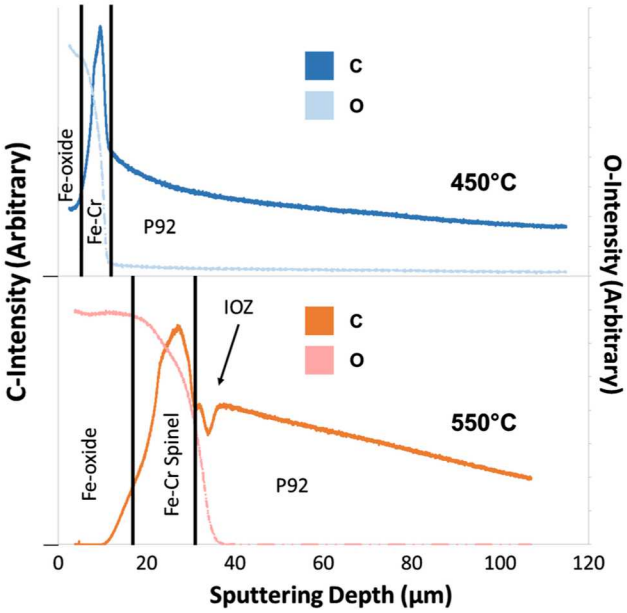

Fig. 8—GD-OES results for P92 samples which were exposed to CO_2 at 20 MPa for 1000 h at 450 °C (top) and 550 °C (bottom). Carbon plotted against left axis, oxygen plotted against the right (both linear scales).

GD-OES was used to analyze the depth profile of carbon from the surface for both CO_2 exposures, see Figure 8, with a depth resolution of roughly 5 μm (based on sputtering depth variation). The depth profiles match those of previous studies of high pressure, static (or pseudo-static) studies.[16] Both exposures revealed little carbon in the outer magnetite, as observed previously.[16,17] Carbon present within magnetite has been shown to decrease with additional corrosion, and this was observed as no carbon was left in magnetite after exposure to 550 °C. The carbon profile then reached a maximum in the inner Fe-Cr spinel. This supports the theory that the outer magnetite grows on the oxide–gas interface, where carbon is not deposited—or, if it is deposited, is quickly oxidized due to the porous growth of the magnetite—while the inner Fe-Cr spinel grows inward, depositing carbon as gaseous CO_2 oxidizes.

Beneath the Fe-Cr spinel, the different temperature exposures resulted in dissimilar carbon profiles. For 550 °C, a local minimum occurred just as the alloy was reached, likely corresponding to the IOZ observed in Figures 1(d) and 3.[16,19] As depth increased in the alloy, carbon content decreased in a linear fashion (observed previously for P91[16]). Conversely, the profile for 450 °C-exposed material decreased in a gradual exponential decay, approximating a concentration gradient typical for diffusion. A decrease in carbon after the oxide has been observed (due to the IOZ),[15] but it was likely too thin for the depth resolution of this analysis. The linear decrease in carbon content within P92 after exposure at 550 °C indicates that the depth of carburization (when the carbon measured is equal to the alloying carbon) is shallower than with the exponential decrease found for 450 °C. This supports the findings of micro-hardness and etching to show that while carburization was more damaging after 550 °C exposure, it was less penetrating than at 450 °C. As we know that there was more carbon deposited at 550 °C, the volume fraction of carbides formed within the carburized region is likely much higher than at similar depths at 450 °C.

IV. DISCUSSION

The study of welded and base material in parallel allowed for an analysis of how the welding process affected the corrosion performance of P92. The results indicate that both oxidation and carburization occurred at a similar rate within all regions: fusion, HAZ, and base. This shows that the welding process and PWHT of P92 maintains the same level of corrosion protection and mechanical property response of base material. Therefore, this work has determined that there is no detrimental corrosion performance due to the similar welding P92, provided the weld is of good quality.

While it has been shown that exposure of P92 and other similar grade steels are susceptible to corrosion in s-CO_2, the results presented here show that specific effects are highly dependent on temperature and pressure, as well as exposure time. Oxidation and mass change analysis showed that there was roughly three times the corrosion (both oxidation and carburization) at 550 °C relative to 450 °C. Small differences between the oxides were observed: hematite at 450 °C but not at 550 °C, and an observable IOZ at 550 °C but not at 450 °C (though an IOZ is assumed to have been present). From these results alone, it could be posited that the performance of P92 at 550 °C represents the results from long-term exposure at 450 °C; that the mechanical properties of the alloy could be correlated to oxide thickness—or, at least, internal oxide thickness—regardless of temperature.

However, carburization analysis contradicts this position. While mass change indicated additional carbon deposition at 550 °C, the depth of carburization was greater at 450 °C. This appears to be due to a confluence of factors: diffusion rates of carbon and Cr at 450 °C *vs* 550 °C; the rate of carbon deposition; and the kinetics of carbide formation. Previous work at 550 °C has shown that $M_{23}C_6$ carbides coarsen along grain boundaries, but near the surface the activity of carbon increases such that the carbon-rich M_7C_3 forms both intra and intergranularly.[16,20] Meanwhile, other work at 450 °C has shown noticeable carburization limited to grain boundary carbide coarsening, likely in the form of $M_{23}C_6$.[15] This study has confirmed that the relationship between the total deposited carbon and carburization depth is dependent on both exposure temperature and rate of internal oxidation (hence, the rate of carburization).

At both 450 °C and 550 °C, internal oxidation and CO recombination liberates free C. The instability of carbides relative to oxides forces the carbon to diffuse into the alloy to bond with metal elements—primarily Cr. These Cr-rich carbides form in islands, or precipitates, directly beneath the oxide, forming the IOZ and continuing the process of duplex oxidation described

above. The oxidation of these islands re-liberates the carbides and forces carbon still deeper into the alloy. Thus, begins a process in which the kinetics for carbide formation (of first $M_{23}C_6$ and then of more carbon-rich phases) and Cr diffusion competes with the rates of carbon deposition from internal oxidation and carbon intergranular diffusion. At 450 °C and 20MPa, this competition was dominated by deposition and diffusion: the IOZ was too small to be observed with SEM and the depth of carburization was >200 μm. However, at 550 °C the carburization process was dominated by precipitation and coarsening of Cr-rich carbides: a thick IOZ and a total carbon enrichment depth of roughly 100 μm. This supports the work on P92 and other steels which indicate faster carburization kinetics at higher temperatures (peaking in the 750-900 °C range).[5,34,35] Therefore, the study of P92 and similar alloys in s-CO_2 should note that the precise temperature and oxidation rate can change the concentration gradient of carbon within the material, even when oxide thicknesses appear similar.

As an example, based on data from previous work,[15] it is projected that P92 exposed at 450 °C for roughly 7500 hours would produce an oxide of 36.9 μm (the thickness seen here after exposure at 550 °C for 1000 hours). This means that roughly the same carbon will have been deposited into the P92 in both conditions (450 °C for 7500 hours, 550 °C for 1000 hours), but the 450 °C exposure will produce a different carbon depth profile. Previous work has shown that at 1000 h the carburization depth increase has slowed significantly compared to the initial 200 or 600 hours.[15] This data can project that the 7500 hours of exposure at 450 °C would produce carburization to a depth of 300–500 μm, forcing the deposited carbon to be 3–5 times more diffuse than observed here after exposure at 550 °C for 1000 hours. This indicates two things: first, that the mechanical effects of carburization in P92 are much more severe at 550 °C than at 450 °C, even when the amount of carbon deposited is equal; and second, that carburization at 450 °C could possibly result in embrittlement within a year (8760 hours). Further work with *in situ* corrosion-assisted crack growth should be performed to measure the impact of this carburization in a more quantifiable manner. However, this work indicates that P92—despite the high performance of its weld—is likely not a material that should be used for pressurized systems of s-CO_2 at or above 450 °C.

V. CONCLUSION

Exposures of P92 in CO_2 at 20 MPa for 1000 hours were completed at temperatures of 450 °C and 550 °C, and a comparative aging study was completed in Ar at 550 °C, 0.02 MPa for 1000 h. Several conclusions were made based on this work:

- Similar values for mass gain and oxide thickness, as well as similar mechanical property responses to exposure, allow for the conclusion that there was no observed difference between welded and base P92.
- Carburization analysis showed that while more carbon was deposited in the 550 °C s-CO_2 environment, 450 °C exposure resulted in roughly twice the depth of attack. The difference in carbon depth profiles was attributed to the interplay of oxidation rate, carbide precipitation and coarsening kinetics, and diffusion rates of carbon and Cr within the alloy.
- While tensile testing showed a detrimental impact from carburization at 550 °C and not at 450 °C, this was ascribed to elevated carbon buildup near the oxide–metal interface at 550 °C functioning as crack initiation sites, while the requisite buildup was not observed at 450 °C.
- Projections indicate that carburization of P92 at 450 °C will equal that seen here for 550 °C exposure after roughly 7500 hours, but the larger depth of carbon ingress will suppress the maximum concentration of carbon near the oxide–metal interface.
- While carbide coarsening had not caused deteriorated mechanical properties at 450 °C after 1000 hours, the effect of additional carbon deposition was not determined. Further study of *in situ* stress creep and fatigue should be completed before implementation of P92 at or above 450 °C.

ACKNOWLEDGMENTS

The author gratefully acknowledges the contributions made to this work by Paul Brooks, Peter Li, and Ryan Carroll at the University of Wisconsin-Madison. Sandia National Laboratories is a multimission laboratory managed and operated by National Technology and Engineering Solutions of Sandia, LLC., a wholly owned subsidiary of Honeywell International, Inc., for the U.S. Department of Energy's National Nuclear Security Administration under Contract DE-NA-00 03525.

FUNDING

This work was supported by Advance supercritical carbon dioxide cycles [DE-EE0007120] and the U.S. Department of Energy.

DATA AVAILABILITY

The raw data used for this work is available upon request from the corresponding author.

REFERENCES

1. V. Dostal: *A Supercritical Carbon Dioxide Cycle for Next Generation Nuclear Reactors*, Massachusetts Institute of Technology, Cambridge, 2004.
2. Y. Kato, T. Nitawaki, and Y. Muto: *Nucl. Eng. Des.*, 2004, vol. 230, pp. 195–207.

3. I. G. Wright, B. A. Pint, J. P. Shingledecker, and D. Thimsen, "Materials Considerations for Supercritical CO2 Turbine Cycles," in *ASME Turbo Expo 2013: Turbine Technical Conference and Exposition*, 2013.
4. R.L. Klueh and A.T. Nelson: *J. Nucl. Mater.*, 2007, vol. 371, pp. 37–52.
5. S.S. Wang, D.L. Peng, L. Chang, and X.D. Hui: *Mater. Des.*, 2013, vol. 50, pp. 174–80.
6. J.C. Vaillant, B. Vandenberghe, B. Hahn, H. Heuser, and C. Jochum: *Int. J. Press. Vessel. Pip.*, 2008, vol. 85, pp. 38–46.
7. A. Vyrostkova, V. Homolova, J. Pecha, and M. Svoboda: *Mater. Sci. Eng. A*, 2008, vol. 480, pp. 89–298.
8. P.J. Ennis, A. Zielinska-Lipiec, O. Wachter, and A. Czyrska-Filemonowicz: *Acta Mater.*, 1997, vol. 45, pp. 4901–07.
9. Y. Gong, D.J. Young, P. Kontis, Y.L. Chiu, H. Larsson, A. Shin, J.M. Pearson, M.P. Moody, and R.C. Reed: *Acta Mater.*, 2017, vol. 130, pp. 361–74.
10. R. Viswanathan and W. Bakker: *J. Mater. Eng. Perform.*, 2001, vol. 10, pp. 81–95.
11. S.G. Hong, W.B. Lee, and C.G. Park: *J. Nucl. Mater.*, 2001, vol. 288, pp. 202–07.
12. M. Taneike, K. Sawada, and F. Abe: *Metall. Mater. Trans. A*, 2004, vol. 35A, pp. 1255–62.
13. S. Kunimitsu, Y. You, N. Kasuya, Y. Sasaki, and Y. Hosoi: *J. Nucl. Mater.*, 1991, vol. 179, pp. 689–92.
14. L. Tan, D. T. Hoelzer, and J. T. Busby, "Microstructure and Basic Mechanical Properties of the Procured Advanced Alloys for the Advanced Radiation Resistant Materials Program," No. ORNL/TM-2014/439, 2014.
15. M.N. Arik: *Corrosion of Ferritic Steels in Supercritical CO2 at 450 °C*, University of Wisconsin-Madison, Madison, 2017.
16. F. Rouillard, G. Moine, M. Tabarant, and J.C. Ruiz: *Oxid. Met.*, 2012, vol. 77, pp. 57–70.
17. F. Rouillard and T. Furukawa: *Corros. Sci.*, 2016, vol. 105, pp. 120–32.
18. D. Young, P. Huczkowski, T. Olszewski, T. Hüttel, L. Singheiser, and W.J. Quadakkers: *Corros. Sci.*, 2014, vol. 88, pp. 161–169.
19. L. Martinelli, C. Desgranges, F. Rouillard, K. Ginestar, M. Tabarant, and K. Rousseau: *Corros. Sci.*, 2015, vol. 100, pp. 253–66.
20. F. Rouillard, G. Moine, L. Martinelli, and J.C. Ruiz: *Oxid. Met.*, 2012, vol. 77, pp. 27–55.
21. M.G.C. Cox, B. McEnaney, and V.D. Scott: *Nature*, 1972, vol. 237, pp. 140–42.
22. G. B. Gibbs, R. E. Pendlebury, and M. R. Wootton, "Protective and breakaway corrosion of mild steel in CO2," in *Proceedings of the British Nuclear Engergy Society International Conference on Corrosion of Steels in CO2*, 1974.
23. R.P. Oleksak, J.H. Tylczak, C.S. Carney, G.R. Holcomb, and O.N. Dogan: *JOM*, 2018, vol. 70, pp. 1527–34.
24. J.T. Mahaffey: *Effect of Partial Pressure of Oxygen and Activity of Carbon on the Corrosion of High Temperature Alloys in s-CO2 Environments*, University of Wisconsin-Madison, Madison, 2017.
25. D.J. Young: *High Temperature Oxidation and Corrosion of Metals*, 1st ed., Elsevier, Amsterdam, 2008.
26. W. Marshall, Z. Zhang, and G. B. Holloway, "Welding Consumables for P92 and T23 Creep Resisting Steels," in *Fifth International EPRI RRAC Conference*, 2002.
27. ASME, "Code Cases - Boilers and Pressure Vessels," in *ASME Boiler and Pressure Vessel Code*, 2015.
28. A.M. Brittan, J. Mahaffey, M. Anderson, and K. Sridharan: *Mater. Sci. Eng. A*, 2019, vol. 742, pp. 414–22.
29. J. Mahaffey, D. Adam, M. Anderson, and K. Sridharan, "Effect of oxygen impurity on corrosion in supercritical CO2 environments," in *The 5th International Supercritical CO2 Power Cycles Symposium*, 2016.
30. J. Mahaffey, D. Adam, A. Brittan, M. Anderson, and K. Sridharan: *Oxid. Met.*, 2016, vol. 86, pp. 567–80.
31. J. D. Tucker, B. Adam, M. Anderson, B. Pint, G. R. Holcomb, C. S. Carney, H. Saari, L. Teeter, J. Mahaffey, O. Dogan, C. Jang, and S. Kung, "Supercritical CO2 round robin test program," in *The 6th International Supercritical CO2 Power Cycles Symposium*, 2018.
32. G. Chen, Q. Zhang, J. Liu, J. Wang, X. Yu, J. Hua, X. Bai, T. Zhang, J. Zhang, and W. Tang: *Mater. Des.*, 2013, vol. 44, pp. 469–75.
33. J.A. Francis, W. Mazur, and H.K.D.H. Bhadeshia: *Mater. Sci. Technol.*, 2006, vol. 22, pp. 1387–95.
34. B. Weiss and R. Stickler: *Metall. Trans.*, 1972, vol. 3, pp. 851–66.
35. F. Penalba, X. Gomez-Mitxelena, J.A. Jimenez, M. Carsi, and O.A. Ruano: *ISIJ Int.*, 2016, vol. 56, pp. 1662–67.